Applied and Computational Mechanics 18 (2024) 189–202

Applied and Computational Mechanics

Numerical analysis of mixed convection and Thomson-Troian slip effects on ternary nanofluid flow and heat transfer over a stretching sheet with porous media: Darcy-Forchheimer model

B. Singh[a], S. Sood[a,*], A. Thakur[b], S. Chandel[a]

[a] *Department of Mathematics and Statistics, Career Point University, Hamirpur (H.P.), India*
[b] *Department of Mathematics, CMR Institute of Technology, Bengaluru, Karnataka, India*

Received 8 April 2024; accepted 30 July 2024

Abstract

The present study unveils research that examines the laminar motion of water-infused nanofluid comprised of nanoparticles of $\mathrm{TiO_2}$ (titanium dioxide), Ag (silver), and Cu (copper) over a stretching sheet. The flow undergoes a novel slip condition based on Thomson and Troian to model complex fluid behavior near solid walls and incorporate the Darcy-Forchheimer model to comprehensively analyze the influence of a porous medium on flow behavior. Moreover, a heat source/sink and radiation are included to ensure the outcome of the energy equation will resemble most actual-world applications. Partial differential equations (PDEs) of higher order, originally used to describe the system are then reformulated into higher-order non-linear ordinary differential equations (ODEs) by taking symmetry variables that are chosen thoughtfully. The resulting boundary layer equations are then turned into a set of ODEs by implementing relevant similarity transformations, which can be solved using the MATLAB function *bvp4c*. Through graphs, the variations in the velocity, Nusselt number, temperature, and skin friction coefficient were displayed. The outcome showed that the incorporation of silver nanoparticles (0.01–0.03) enhanced the skin friction coefficient by $\approx 1.68\,\%$ and the Nusselt number reduced up to $\approx 5\,\%$. The Forchheimer number also reported a 6.5% enhancement and 1.5% reduction in the skin friction coefficient and the Nusselt number, respectively. The velocity slip parameter γ_1 correlates with an upswing in temperature and skin friction coefficient for the ternary nanofluid while observing a decline in the velocity and Nusselt number.

Keywords: Darcy-Forchheimer model, linearly stretching sheet, ternary nanofluid, thermal radiation, porous media

1. Introduction

The study of nanofluids has grown to be a significant research area due to its many uses for the manufacture of mineral-based oils, liquids, solar energy and electronic devices. More than two decades have passed since the investigation of a novel class of functional fluids in use, termed nanofluids [5]. The terminology "nanofluids" was initiated by Choi in 1995 to characterize fluids harboring dispersed nanoparticles [49]. Nanofluids, which are produced by dispersion nanomaterials within ordinary fluid heat-transferring fluids, are proposed as the upcoming phase of heat-transferring fluids as they provide intriguing novel possibilities for enhancing the effectiveness of heat transmission in comparison to average fluids [41]. A fluid obtained when either metallic or non-metallic nanoparticles, nanotubes, nanofibers, or nanowires possessing an average size below 100 nm are dispersed in a liquid, is known as a nanofluid. Oil, ethylene glycol, water and propylene glycol are a few examples of heterogeneous combinations of both liquid and solid forms that collectively make up a nanofluid [28]. Small particles (metal (Cu,

*Corresponding author. Tel.: +91 981 628 08 85, e-mail: shilpasood221188@gmail.com.
https://doi.org/10.24132/acm.2024.894

Ag, Au), carbon (graphene, diamond, graphite, fullerene, carbon nanotube) or metal oxides (TiO_2, Al_2O_3, ZrO_2, SiO_2, CuO)) constitute the solids in this specific instance [6, 27]. This mixture establishes a colloidal solution in constant situations, with or without the presence of dispersion agents. Nanofluids have recently garnered a lot of attention due to their significantly improved thermal characteristics [12, 17, 23]. Nanofluids offer the capacity to decrease the thermal barriers, and the industrial sectors that could profit from comparable enhanced heat transfer fluids are very diverse [46, 50]. An additional inactive method of enhancing heat transfer that has drawn a lot of interest from academics and researchers is the utilization of nanofluids as a channel for heat transfer. Its unique transport characteristics distinguish it from a base fluid and make it the ideal operating fluid for all heat transfer devices. Increased heat transfer properties of a solid-liquid stage combination are generally caused by suspended particles of solids with greater thermal conductivity in the main fluid. As a result of its special cooling properties, a nanofluid has been applied in every science and technology phase, including thermal storage, solar energy conversion (solar cells, solar stills), HVAC (Heating, Ventilation, and Air Conditioning) systems, tubes for heating structures, space and defense, healthcare, vehicles, radiators, nuclear-powered reactor cores and photovoltaic thermal systems (PV/T) [8, 9, 30, 34].

Hybrid and tri-hybrid nanofluids are the latest varieties of fluid made from nanocomposite technology that are excellent at transmitting energy [14]. In recent years, investigators and researchers have produced a pioneering nanofluid, by adding nanoparticles of three dissimilar kinds into the finest fluid. A tri-hybrid or ternary nanofluid (THNF) denotes this revolutionary nanofluid. The increased need for cooling agents in the mixture of its excellent thermal potential at the level of manufacturing has occupied scientists to improve the current nanofluid, owing to this fact THNF has undergone the improvement of thermal properties [18]. THNF has several interesting characteristics. Investigators are very interested in THNFs because of their exceptional thermophysical properties. When it comes to their capacity for heat transport, THNFs are superior to mono and hybrid nanofluids [47]. In [31], Mousavi et al. investigated the heterogeneous THNFs of titanium oxide, copper oxide, and magnesium oxide. Algehyne et al. [3] investigated the transfer of energy via a THNFs flow over an extended permeable barrier made up of MgO, TiO_2, and $CoFe_2O_4$ nanoparticles.

Darcy is acknowledged for developing the concept of fluid flow over porous media. However, due to its disadvantages—lower porosity and lesser velocity—this idea would not have been as widely recognized. To resolve the evident deficit, Forchheimer modified the momentum model by adding a quadratic velocity component. Later on, Muskat labeled this component "the Forchheimer term" [15]. The Darcy-Forchheimer model was addressed by Pal and Mondal who arrived at the conclusion that a high electric field causes the fluid's volume to decrease using porous materials across a continuously expanded surface [35]. In [37], Rooman et al. examined velocity and heat transport in the context of the Darcy-Forchhemier model for the THNFs of TiO_2, Al_2O_3, and SiO_2. Gul et al. [19] investigated the enhancement of heat movement for the Darcy-Forchheimer THNF of TiO_2, $CoFe_2O_4$ and MgO/H_2O. In [11], Dero et al. studied the 3D magnetized device using the Darcy-Forchheimer movement across a decreasing area of the $Cu + Al_2O_3/H_2O$ hybrid nanofluid (HNF). In [45], Tlili et al. analyzed the persistent 3D Eyring-Powell nanoliquid flow across an uneven stretchable Darcy-Forchheimer sponge substrate, employing entropy generation analysis. The outcome suggests a marked reduction in liquid velocity by alterations in the Darcy-Forchheimer number (Fr).

Selection of an appropriate boundary condition is crucial during the modulation of fluid flow. One of the simplest and most commonly used boundary conditions is the no-slip condition. This condition dictates that a liquid element adjacent to the surface assumes the velocity of

the surface [10]. Unlike the no-slip condition, the Navier slip condition allows for a finite slip velocity at the boundary, where the slip velocity depends linearly on the shear stress. The Navier slip condition accommodates a range of slip behaviors by adjusting the slip length parameter, making it versatile for different fluid-solid interactions [33]. The Thompson and Troian slip condition can be considered as a more generalized form of the classical Navier slip condition. While the Navier slip condition assumes a linear relationship between the slip velocity and the shear rate at the boundary, the Thompson and Troian slip condition introduces a non-linear dependence on the shear rate [44].

In [25], Li et al. examined a THNF, which is produced by holding nanoparticles of three distinct types: $\mathrm{TiO_2}$, Cu, and $\mathrm{Ag/H_2O}$, and evaluated it past an extended sheet under the influence of slip constraints according to Thomson and Troian. The study findings showed temperature enhancement but reduced flow velocity with nanoparticle suspension due to density effects. The stagnation region movement of carbon nanoliquids paired to a generated magnetic field over a Riga surface with the inclusion of the Troian and Thomson slip conditions is studied in [32]. Ahmad and Nadeem addressed in their work [1] the reduction of entropy in the stagnation point dynamics of an HNF over a porous medium's non-linear and permeable stretching sheet under the Thomson and Troian slip circumstances. The results showed that HNF with carbon nanotubes enhanced thermal conductivity and heat transfer performance more effectively than a simple nanofluid. Subject to the Thomson and Troian boundary conditions and taken into account within the Darcy-Forchheimer porous media, Akaje [2] examined the impact of nonlinear radiative warmth on specific heat exchange in a magnetohydrodynamic (MHD) Casson nanofluid at a stagnation point. The medium temperature is shown to decrease with an elevated thermal relaxation parameter based on the obtained results, while greater heat transfer is noted with expanded temperature proportion heating radiation, Biot number, Eckert number, and Casson variable. In [29], Mishra investigated the electromagnetic and thermal characteristics of THNF flowing over a permeable plate by considering the Thomson and Troian slip, suction/blowing, and chemical reaction effects. The skin friction coefficient and Nusselt number were found to be greatly impacted by changes in the velocity slip parameter, underscoring the parameter's crucial significance in the dynamics of fluid flow and heat transfer. Xin et al. [48] examined the impact of Joule heating and viscous dissipation on the thermal performance of Williamson nanofluid under the Thompson and Troian slip conditions. The results indicated that higher thermophoresis and Brownian motion parameters enhance heat conduction, increased Eckert numbers boost nanofluid temperature, and Lorentz forces regulate flow velocity.

Despite the advancements in understanding nanofluid behavior, a research gap exists in exploring the flow characteristics of $\mathrm{Ag–Cu–TiO_2/H_2O}$ THNF over a stretched sheet, particularly under the Thomson and Troian slip parameters and within porous media. Therefore, utilizing the Darcy-Forchheimer model (for porous media), the authors have thought about analyzing the fluid motion and the exchange of heat characteristics under the influence of slip constraints of the nanofluid generated from a base fluid (water) with suspended nanoparticles (Ag, Cu, and $\mathrm{TiO_2}$). This investigation seeks to evaluate and clarify the effects associated with these conditions. The governing partial differential equations (PDEs) for flow and heat distribution are first transformed into a set of self-similar nonlinear ordinary differential equations (ODEs) using the similarity solution technique. The reduced coupled ODEs are mathematically solved using the MATLAB *bvp4c* approach. The resulting data is then visualized in figures and tables, which are used to discuss the physical effects of varying parameters on the system.

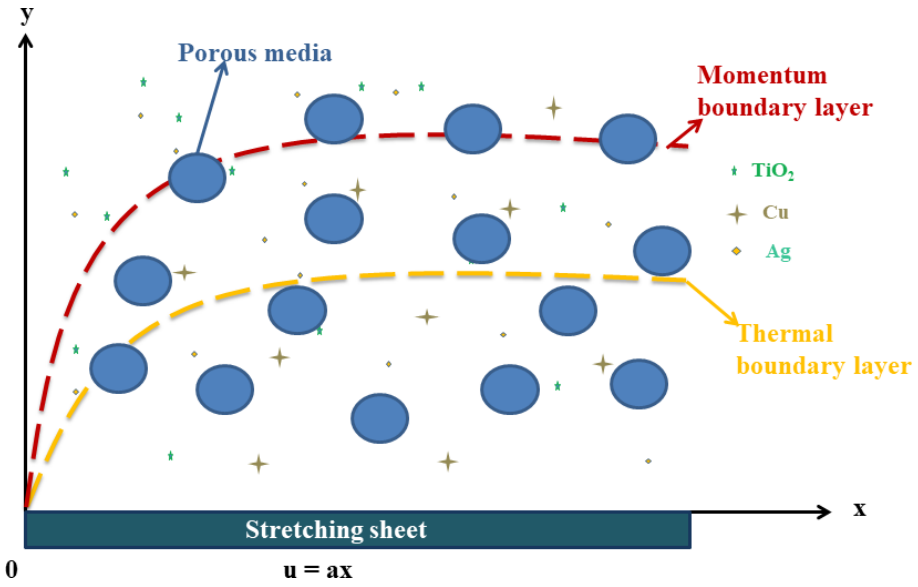

Fig. 1. Flow arrangement

2. Mathematical description of the problem

Let us consider a situation where a ternary nanofluid containing TiO_2, Cu, and Ag nanoparticles in water experiences a two-dimensional laminar flow. This fluid flows over a horizontally stretched sheet (Fig. 1), with $u_w = ax$ as velocity, and along the respective y- and x-axes, the flow is characterized by the v- and u-components. The Thomson and Troian slip conditions, along with temperature slip at the sheet surface, are considered. Heat generation, Darcy-Forchheimer effects, and mixed convection are also taken into account. The governing equations, boundary layer approximation, and the impact of radiation effects can be written as follows [25, 26]:

$$\frac{\partial u}{\partial x} + \frac{\partial v}{\partial y} = 0, \tag{1}$$

$$u\frac{\partial u}{\partial x} + v\frac{\partial u}{\partial y} = \nu_{tf}\frac{\partial^2 u}{\partial y^2} + \frac{g\,(\varrho\beta)_{tf}}{\varrho_{tf}}\,(T - T_\infty) - \frac{\nu_{tf}}{k^*}u - Fu^2, \tag{2}$$

$$u\frac{\partial T}{\partial x} + v\frac{\partial T}{\partial y} = \alpha_{tf}\frac{\partial^2 T}{\partial y^2} + \frac{Q_0}{(\varrho C_p)_{tf}}\,(T - T_\infty) - \frac{1}{(\varrho C_p)_{tf}}\frac{\partial q_r}{\partial y}. \tag{3}$$

The kinematic viscosity is expressed as $\nu = \mu/\rho$, $F = C_b/[x(k^*)^{1/2}]$ is the medium variable inertia coefficient, where k^* is the permeability of the porous medium denoted by T, the temperatures T_∞ and T_w correspond to ambience and surface. Further, ρ_{tf}, β_{tf}, ν_{tf}, and $(\rho C_p)_{tf}$ denote the nanofluid effective density, thermal expansion coefficient, kinematic viscosity, and heat capacitance. The subscript 'tf' indicates tri-hybrid nanofluid.

Selecting H_2O as the fundamental fluid proves advantageous owing to its inherent optical thickness, allowing for the effective utilization of the Rosseland approximation to model radiation as [2]

$$q_r = -\frac{4\sigma^*}{3K^*}\frac{\partial T^4}{\partial y}, \tag{4}$$

where σ^* and K^* represent the Stefan-Boltzmann term and the mean absorption coefficient.

With due consideration, the specified boundary conditions [44] are formulated as follows

$$u = u_w + u_1 \frac{\partial u}{\partial y}\left(1 - u_2 \frac{\partial u}{\partial y}\right)^{-\frac{1}{2}}, \quad v = 0, \quad T = T_w + L\frac{\partial T}{\partial y} \quad \text{at } y = 0, \\ u \to 0, \quad T \to T_\infty \quad \text{as } y \to \infty, \tag{5}$$

where u_1 represents the Navier slip length density and u_2 is the reciprocal of some critical shear rate. Employing a similarity transformation [7] as follows

$$u = \frac{\partial \psi}{\partial y},\ v = -\frac{\partial \psi}{\partial x},\ v = -\sqrt{a\nu_f}F(\eta),\ u = axF'(\eta),\ \eta = y\sqrt{\frac{a}{\nu_f}},\ \theta(\eta) = \frac{T - T_\infty}{T_w - T_\infty}, \tag{6}$$

the PDEs are altered into an ODEs set, where the stream function is defined as $\psi(x, y) = \sqrt{a\nu_f}xF(\eta)$ and the system of equations obtained is

$$\frac{\mu_{tf}}{\mu_f}F''' + \frac{\varrho_{tf}}{\varrho_f}\left[FF'' - (F')^2\right] + \lambda\frac{(\varrho\beta)_{tf}}{(\varrho\beta)_f}\theta - \lambda_1 F'\frac{\varrho_{tf}}{\varrho_f} - Fr(F')^2\frac{\varrho_{tf}}{\varrho_f} = 0, \tag{7}$$

$$\left(\frac{K_{tf}}{K_f} + \frac{4}{3}R\right)\theta'' + \text{Pr}\left[\frac{(\varrho C_p)_{tf}}{(\varrho C_p)_f}F\theta' + Q\theta\right] = 0. \tag{8}$$

The form of the related boundary conditions is as follows

$$F(0) = 0,\ F'(0) = 1 + \gamma_1\frac{F''}{\sqrt{1 - \gamma_2 F''}},\ \theta(0) = 1 + T_s\theta',\ F'(\infty) \to 0,\ \theta(\infty) \to 0. \tag{9}$$

The expressions provided below represent the quantities of physical significance after undergoing a transformation,

$$Cf_x\sqrt{\text{Re}_x} = \frac{\mu_{tf}}{\mu_f}F''(0) \quad \text{and} \quad \frac{\text{Nu}_x}{\sqrt{\text{Re}_x}} = -\frac{K_{tf}}{K_f}\left(1 + \frac{4}{3}R\right)\theta'(0). \tag{10}$$

The non-dimensional parameters that are taken under consideration during the transformation of the system of equations are

$$\lambda = \frac{g\beta_f(T_w - T_\infty)}{a^2 x}, \quad \text{Pr} = \frac{\nu_f}{\alpha_f}, \quad R = \frac{4\sigma^* T_\infty^3}{k^* k_f}, \quad Q = \frac{Q_0}{a(\varrho C_p)_f}, \quad \gamma_1 = u_1 a\sqrt{\frac{a}{\nu_f}}, \\ \gamma_2 = u_2^* ab\sqrt{\frac{a}{\nu_f}}, \quad u_2(x) = \frac{b}{x}u_2^*, \quad T_s = L\sqrt{\frac{a}{\nu_f}}, \quad \lambda_1 = \frac{\nu_{tf}}{ak}, \quad \text{Fr} = \frac{c_b}{K^{1/2}}.$$

3. Solution procedure and validation

The solution of the system of non-linear ODEs (7)–(8) has been accomplished, taking into account the prescribed boundary conditions (9) through the effective utilization of the *bvp4c* numerical technique in MATLAB [20, 38–40]. One of the primary merits of employing this method is its proficiency in solving multipoint boundary value problems (BVPs), a capability that distinguishes it from most other methods available. Furthermore, it offers a user-friendly interface for source code modification, making it adaptable to a wide range of problem types. For the solution achieved, a new conversion is discussed as follows:

Table 1. A comparison of the findings related to $-\theta'(0)$

Pr	Present result	Gorla and Sidwai [36]	Khan and Pop [24]	Hamad [21]
0.70	0.453 9	–	0.453 9	0.453 9
2	0.911 4	0.911 4	0.911 3	0.911 3
6.13	1.759 7	1.759 6	1.759 7	–
7	1.895 4	1.895 4	1.895 4	1.895 4
20	3.353 9	3.353 9	3.353 9	3.353 9

We are introducing novel variables and embedding them within the equations to refine our analysis,

$$F = f(1), \quad F' = f(2), \quad F'' = f(3), \quad \theta = f(4), \quad \theta' = f(5). \tag{11}$$

Incorporating the newly introduced variables into the equation set (7)–(8) results in the derivation of a system of first order equations

$$\begin{aligned}
f'(1) &= f(2),\\
f'(2) &= f(3),\\
f'(3) &= \frac{\mu_f}{\mu_{tf}}\left[\lambda_1 f(2)\frac{\varrho_{tf}}{\varrho_f} + \mathrm{Fr} f(2)^2\frac{\varrho_{tf}}{\varrho_f} - \lambda f(4)\frac{(\varrho\beta)_{tf}}{(\varrho\beta)_f} - \frac{\varrho_{tf}}{\varrho_f}\left(f(1)f(3) - f(2)^2\right)\right],\\
f'(4) &= f(5),\\
f'(5) &= -\mathrm{Pr}\left[\frac{(\varrho C_p)_{tf}}{(\varrho C_p)_f} f(1)f(5) + Q f(4)\right]\left(\frac{K_{tf}}{K_f} + \frac{4}{3}R\right)^{-1}.
\end{aligned} \tag{12}$$

The boundary conditions (9) transform into

$$fa(1) = 0,\ fa(2) = 1 + \gamma_1\frac{f(3)}{\sqrt{1-\gamma_2 f(3)}},\ fa(4) = 1 + T_s fa(5),\ fb(2) = 0,\ fb(4) = 0.$$

In conclusion, we solve the first order system of equations under the influence of boundary conditions using the MATLAB software. We fine-tune the initial approximations, step size, and position of the boundary layer edge for accuracy assurance. The current study aligns well with findings from prior publications. To ensure accuracy, the obtained solutions are cross-validated (for the Prandtl number Pr) against the existing literature results, demonstrating a consistent match, as summarized in Table 1.

4. Results and discussion

This section contains a thorough review and assessment of our *bvp4c* method-derived results. These results are systematically documented in tables and graphs, providing insight into the intricate behavior of the ternary nanofluid Ag–Cu–$\mathrm{TiO_2}/\mathrm{H_2O}$, where Tables 2 and 3 show the expression for distinct characteristics of these nanoparticles and thermal properties of nanofluid. The visual depiction of important fluid flow characteristics, such as the radiation parameter (R), the concentration of nanoparticles (ϕ), the mixed convection parameter (λ), and the Forchheimer number (Fr), is captured in Figs. 2–5, as well as the velocity slip parameter (γ_1) and the local porosity parameter (λ_1). Examining the temperature, local Nusselt number, nanoliquid velocity,

Table 2. Tri-hybrid nanofluid characteristics related to heat and physical behavior [4, 43]

Properties	Tri-hybrid nanofluid
Density	$\varrho_{tf} = (1-\phi_1)(1-\phi_2)[(1-\phi_3)\varrho_f + \phi_3\varrho_3] + \phi_2\varrho_2 + \phi_1\varrho_1$
Viscosity	$\mu_{tf} = \dfrac{\mu_f}{(1-\phi_1)^{2.5}(1-\phi_2)^{2.5}(1-\phi_3)^{2.5}}$
Thermal conductivity	$\dfrac{k_{tf}}{k_{hnf}} = \dfrac{k_1 + (n-1)k_{hnf} - (n-1)\phi_1(k_{hnf}-k_1)}{k_1 + (n-1)k_{hnf} + \phi_1(k_{hnf}-k_1)}$
Thermal expansion coefficient	$(\varrho\beta)_{tf} = (1-\phi_1)(1-\phi_2)[(1-\phi_3)(\varrho\beta)_f + \phi_3(\varrho\beta)_3] + \phi_2(\varrho\beta)_2 + \phi_1(\varrho\beta)_1$
Heat capacity	$(\varrho C_p)_{tf} = (1-\phi_1)(1-\phi_2)\left[(1-\phi_3)(\varrho C_p)_f + \phi_3(\varrho C_p)_3\right] + \phi_2(\varrho C_p)_2 + \phi_1(\varrho C_p)_1$

Table 3. Nanoparticles and base liquid physical characteristics [13, 22]

Parameters	TiO_2	Cu	Ag	H_2O
$\varrho\,[\mathrm{kg\,m^{-3}}]$	4 250	8 933	10 500	997.1
$K\,[\mathrm{W\,m^{-1}\,K^{-1}}]$	8.953	401	429	0.607 1
$C_p\,[\mathrm{J\,kg^{-1}\,K^{-1}}]$	686.2	385	235	4179
$\beta \times 10^{-5}\,[\mathrm{K^{-1}}]$	0.9	1.67	1.89	21

and skin friction coefficient for the aforementioned flow-related variables is intended. Table 4 demonstrates how changing different parameters affects the values of $F''(0)$, $\theta'(0)$ ($\lambda = 1.0$, $T_s = 0.6$, $Q = -0.2$, Pr $= 6.2$, $\phi_1 = \phi_2 = 0.01$, $\gamma_2 = 0.4$, and $\lambda_1 = 0.5$). The results indicate that ϕ_3 (0.01–0.03) enhances the skin friction coefficient by approximately 1.68 % and reduces the Nusselt number by up to 5 %. Additionally, Fr is associated with a 6.5% increase in the skin friction coefficient and a 1.5% decrease in the Nusselt number. By contrast, an increase in R

Table 4. Variation in $-F''(0)$ and $-\theta'(0)$ with distinct variables

R	γ_1	ϕ_3	Fr	$-F''(0)$	$-\theta'$
0.8	0.2	0.01	0.5	0.943 3	0.714 9
		0.02		0.968 2	0.708 8
		0.03		0.990 8	0.702 9
	0.4			0.785 1	0.687 3
	0.6			0.649 3	0.675 9
	0.8			0.553 2	0.667 4
0.2	0.2			1.022 7	0.803 3
0.4				1.011 0	0.764 5
0.6				1.000 4	0.731 5
0.8			1.0	1.067 9	0.697 8
			1.5	1.137 3	0.687 3

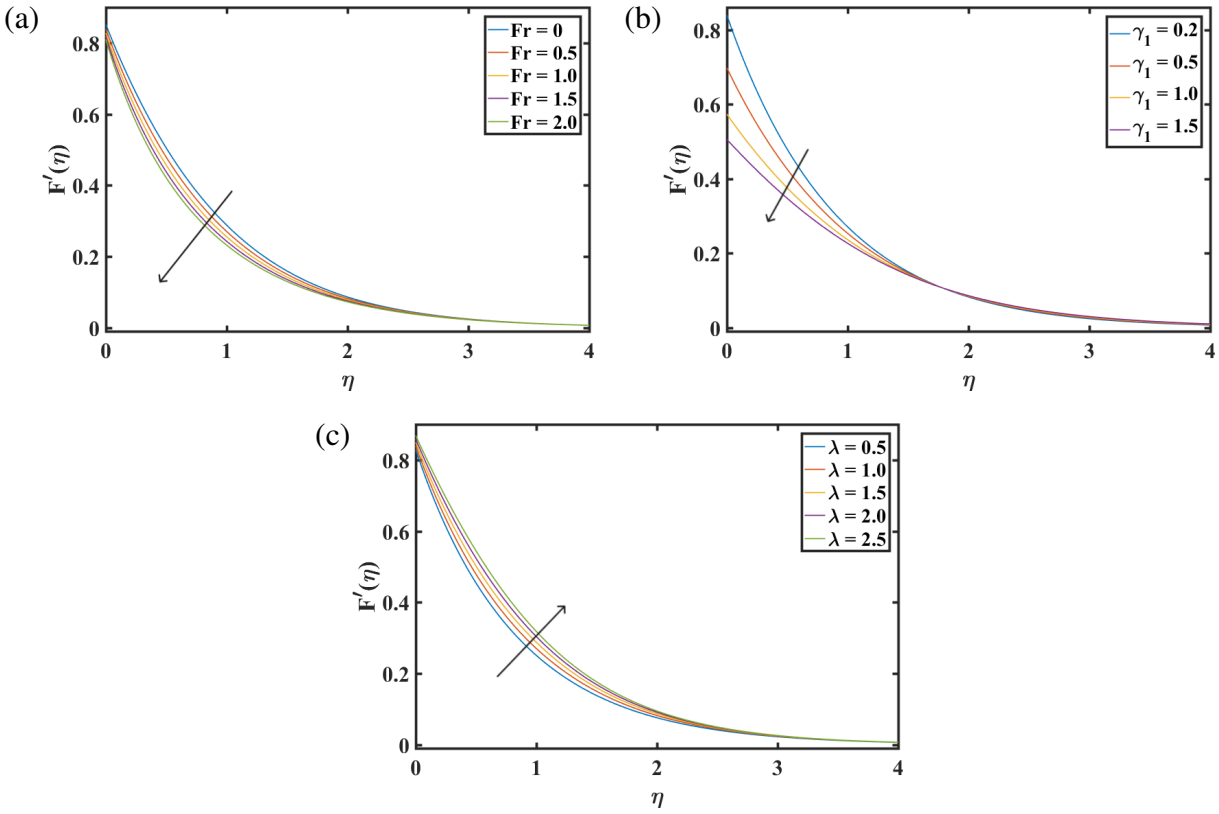

Fig. 2. The dependence of $F'(\eta)$ on (a) Fr, (b) γ_1, and (c) λ

and γ_1 significantly reduces both the skin friction coefficient and the Nusselt number.

Fig. 2 presents the variation in the velocity profile with Fr, γ_1, and λ. The Forchheimer number describes the relative significance of inertial vs. viscous effects in porous medium flow. From Fig. 2a, it is apparent that when the Fr parameter increases (0–2.0), there is a decrease in the velocity of nanofluid ($\mathrm{Ag–Cu–TiO_2/H_2O}$). Higher Forchheimer numbers indicate a greater emphasis on the drag force, which opposes flow and results in lower fluid velocity. Fig. 2b represents the behavior of velocity corresponding to γ_1. It was found out that the velocity slip parameter elevation slowed down the nanofluid movement. Fig. 2c demonstrates the impact of raising the convection parameter (λ) on nanofluid flow. When λ increases, there is a noticeable increase in the velocity of the nanofluid flow. An increased mixed convection parameter leads to greater buoyant force, implying a significant enhancement in the velocity profile magnitude [42].

With the increase in R (0.2–1.0), see Fig. 3a, the temperature within the ternary nanofluid is undergoing an upward trend. This effect is attributed to the enhanced heat input to the fluid during the radiation process, which improves the distribution of temperature across the fluid. This insight is well aligned with published information and highlights thermal radiation particularly in applications where precise control of temperature profiles is critical, such as in thermal management systems and industrial processes [1]. Fig. 3b shows elevation in the thermal profile with the elevation in the velocity slip parameter ($\gamma_1 = 0.2, 0.5, 1.0, 1.5$). It is clear from Fig. 3c that with the increase in the porosity parameter (λ_1 ranging from 0 to 2.0), the temperature profile also rises. A rise in porosity enables a larger fluid volume to traverse the medium, facilitating heat transfer and contributing to an elevation in the overall temperature.

In relation to λ, Fig. 4a illustrates variations in the lowered Nusselt number, $\mathrm{Nu}(\mathrm{Re}_x)^{-1/2}$,

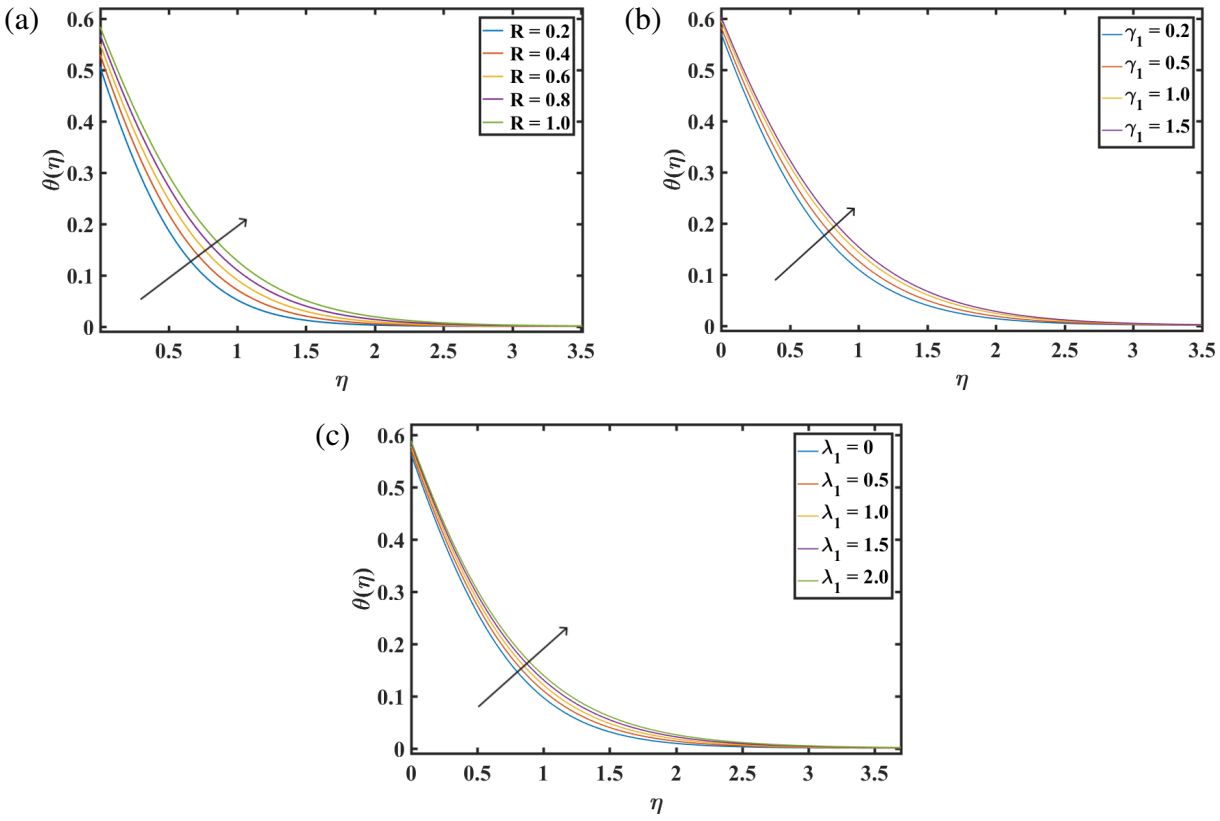

Fig. 3. The dependence of $\theta(\eta)$ on (a) R, (b) γ_1, and (c) λ_1

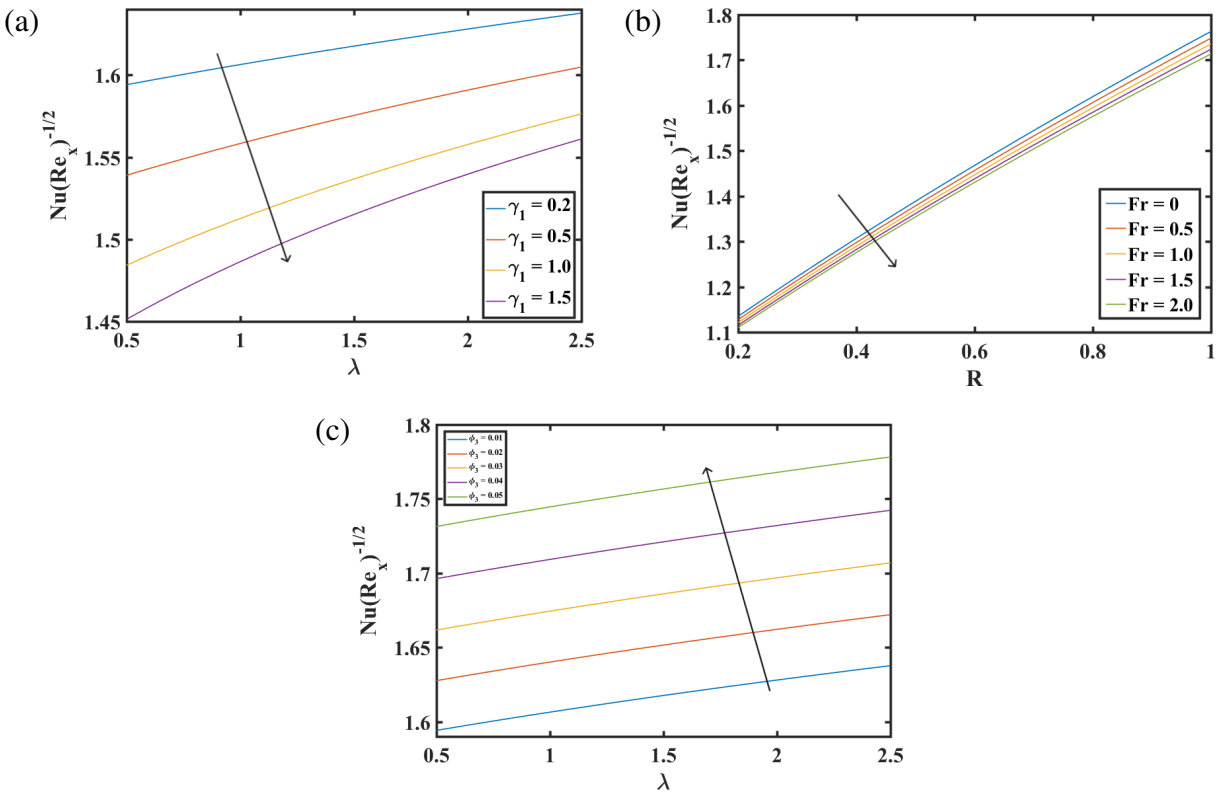

Fig. 4. The dependence of $\mathrm{Nu}(\mathrm{Re}_x)^{-1/2}$ on (a) γ_1, (b) Fr, and (c) ϕ_3

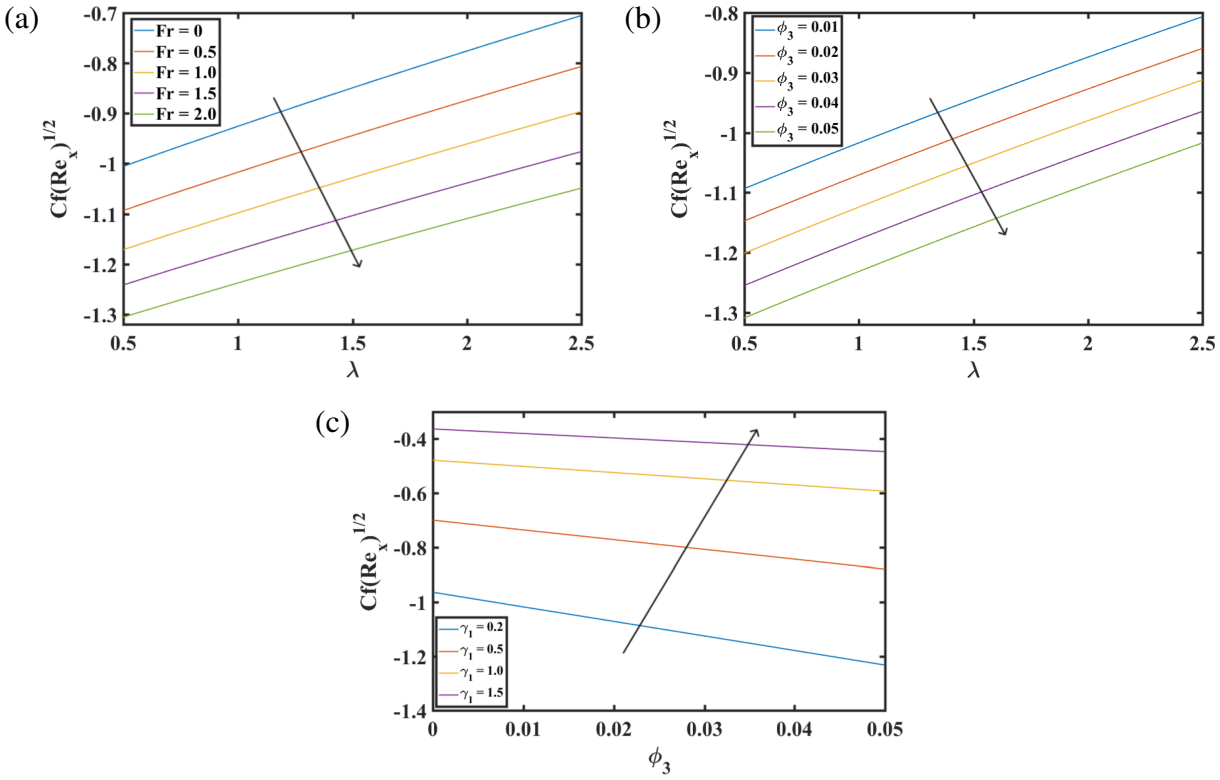

Fig. 5. The dependence of $Cf(\mathrm{Re}_x)^{1/2}$ on (a) Fr, (b) ϕ_3, and (c) γ_1

when γ_1 has a specific level (0.2–1.5). The heat transmission is reduced with the elevation in γ_1 value. Fig. 4b is plotted for $\mathrm{Nu}(\mathrm{Re}_x)^{-1/2}$ against R. Elevated Fr values are linked to a lesser alteration in the reduced Nusselt number, whereas this alteration becomes more prominent with a rise in the parameter R. The consequences of varying nanoparticle volume composition (ϕ_3) and λ on heat transfer are graphically captured in Fig. 4c. The improved value of the Nusselt number helps the fluid to dissipate heat from a heated surface to the surrounding fluid more effectively, hence the nanofluid experiences a synergistic boost in heat transfer efficiency as higher nanoparticle concentration (ϕ_3) facilitates intensified heat conduction, complemented by increased fluid motion driven by mixed convection (λ).

The behavior of the reduced skin friction, $Cf(\mathrm{Re}_x)^{1/2}$, is effectively illustrated in Fig. 5. Fig. 5a–b serves as a visual guide to understanding how the reduced skin friction responds to changes in the convection parameter for different Fr (Fr $= 0, 0.5, 1.0, 1.5, 2.0$) and ϕ_3 ($\phi_3 = 0.01, 0.02, 0.03, 0.04, 0.05$) values, Fig. 5a–b. In both these graphs, the same trend can be observed, in which the value of $Cf(\mathrm{Re}_x)^{1/2}$ decreases with an increase in the parameters Fr and ϕ_3, respectively, with an increasing factor corresponding to λ. With an elevation in ϕ_3, a decreasing trend is noted for skin friction which correlates with results published in [16]. Higher values of the parameter γ_1 are found to enhance the change in $Cf(\mathrm{Re}_x)^{1/2}$, as shown in Fig. 5c.

5. Conclusions

In this research paper, computational numerical modeling is performed for the two-dimensional laminar movement of a ternary nanofluid $\mathrm{Ag–Cu–TiO_2/H_2O}$ over a horizontally extending sheet. The model incorporates the innovative Thomson and Troian slip conditions to simulate complex fluid behavior. Additionally, we integrate the Darcy-Forchheimer model and mixed

convection for a thorough investigation of the impact of the porous medium on flow dynamics. We implemented the *bvp4c* technique in MATLAB for our problem solution. The precision of our findings has been ensured by the careful adjustment of boundary layer parameters and initial approximations, which is in line with prior research. The primary conclusions drawn from this study are:

1. The combined effects of ternary nanofluids, porous media, and mixed convection offer a unique approach to regulating heat transfer characteristics. The presence of multiple nanoparticles (TiO_2, Cu, and Ag) intensifies thermal conductivity within the nanofluid, while the porous medium introduces additional thermal resistance. Mixed convection, arising from buoyancy forces and the stretching sheet motion, further influences heat transfer behavior.
2. The Thomson-Troian slip velocity can lead to higher drag on heat exchanger surfaces while reducing heat transfer efficiency. This translates to increased pumping power requirements due to the higher drag and lower cooling/heating capacity of the heat exchanger due to the reduced heat transfer.
3. The presence of a porous medium results in a reduction of the momentum boundary layer and inflation in the thermal boundary layer. Additionally, the Forchheimer number is associated with a 6.5% increase in the skin friction coefficient and a 1.5% decrease in the Nusselt number.
4. We studied the behavior of the skin friction coefficient of the nanofluid with ϕ_3 (concentration of silver nanoparticles). Here the concentration of Ag is considered because of its high thermal conductivity. Incorporating silver nanoparticles (0.01–0.03) results in an increase about 1.68 % in the skin friction coefficient and a reduction in the Nusselt number by up to 5 %.
5. Complex trends can be seen in the lowered Nusselt number, which increases with larger nanoparticle volume percentage (ϕ_3) and mixed convection parameter (λ).

References

[1] Ahmad, S., Nadeem, S., Flow analysis by Cattaneo-Christov heat flux in the presence of Thomson and Troian slip condition, Applied Nanoscience 10 (2020) 4 673–4 687. https://doi.org/10.1007/s13204-020-01267-4

[2] Akaje, W., Olajuwon, B. I., Impacts of nonlinear thermal radiation on a stagnation point of an aligned MHD Casson nanofluid flow with Thompson and Troian slip boundary condition, Journal of Advanced Research in Experimental Fluid Mechanics and Heat Transfer 6 (1) (2021) 1–15.

[3] Algehyne, E. A., Alrihieli, H. F., Bilal, M., Saeed, A., Weera, W., Numerical approach toward ternary hybrid nanofluid flow using variable diffusion and non-Fourier's concept, ACS Omega 7 (33) (2022) 29 380–29 390. https://doi.org/10.1021/acsomega.2c03634

[4] Alharbi, K. A. M., Ahmed, A. E.-S., Ould Sidi, M., Ahammad, N. A., Mohamed, A., El-Shorbagy, M. A., Bilal, M., Marzouki, R., Computational valuation of Darcy ternary-hybrid nanofluid flow across an extending cylinder with induction effects, Micromachines 13 (4) (2022) No. 588. https://doi.org/10.3390/mi13040588

[5] Alshehri, A., Shah, Z., Computational analysis of viscous dissipation and Darcy-Forchheimer porous medium on radioactive hybrid nanofluid, Case Studies in Thermal Engineering 30 (2022) No. 101728. https://doi.org/10.1016/j.csite.2021.101728

[6] Alwan, M. S., Experimental study for the thermal conductivity of micro and nano fluids by using copper and titanium oxide, University of Thi-Qar Journal for Engineering Sciences 10 (2) (2019) 8–16. https://doi.org/10.31663/tqujes.10.2.192(2019)

[7] Ames, W. F., Nonlinear partial differential equations in engineering, Academic Press, 1965.

[8] Awais, M., Ullah, N., Ahmad, J., Sikandar, F., Ehsan, M. M., Salehin, S., Bhuiyan, A. A., Heat transfer and pressure drop performance of nanofluid: A state-of-the-art review, International Journal of Thermofluids 9 (2021) No. 100065. https://doi.org/10.1016/j.ijft.2021.100065

[9] Darani, K. K., Mozafari, M. R., Supercritical fluids technology in bioprocess industries: A review, Journal of Biochemical Technology 2 (1) (2009) 144–152.

[10] Day, M. A., The no-slip condition of fluid dynamics, Erkenntnis 33 (1990) 285–296. https://doi.org/10.1007/BF00717588

[11] Dero, S., Shaikh, H., Talpur, G. H., Khan, I., Alharbim, S. O., Andualem, M., Influence of a Darcy-Forchheimer porous medium on the flow of a radiative magnetized rotating hybrid nanofluid over a shrinking surface, Scientific Reports 11 (1) (2021) No. 24257. https://doi.org/10.1038/s41598-021-03470-x

[12] Dey, D., Kumar, P., Samantaray, S., A review of nanofluid preparation, stability, and thermophysical properties, Heat Transfer – Asian Research 46 (8) (2017) 1 413–1 442. https://doi.org/10.1002/htj.21282

[13] Divya, S., Alessa, N., Eswaramoorthi, S., Loganathan, K., Thermally radiative Darcy-Forchheimer flow of $\mathrm{Cu/Ag}$ nanoliquid in water past a heated stretchy sheet with magnetic and viscous dissipation impacts, Symmetry 15 (1) (2023) No. 16. https://doi.org/10.3390/sym15010016

[14] Elsebaee, F. A. A., Bilal, M., Mahmoud, S. R., Balubaid, M., Shuaib, M., Asamoah, J. K. K., Ali, A., Motile micro-organism based trihybrid nanofluid flow with an application of magnetic effect across a slender stretching sheet: Numerical approach, AIP Advances 13 (3) (2023) No. 035237. https://doi.org/10.1063/5.0144191

[15] Farooq, U., Hussain, M., Ijaz, M. A., Khan, W. A., Farooq, F. B., Impact of non-similar modeling on Darcy-Forchheimer-Brinkman model for forced convection of Casson nano-fluid in non-Darcy porous media, International Communications in Heat and Mass Transfer 125 (2021) No. 105312. https://doi.org/10.1016/j.icheatmasstransfer.2021.105312

[16] Ghadikolaei, S. S., Yassari, M., Sadeghi, H., Hosseinzadeh, K., Ganji, D. D., Investigation on thermophysical properties of $\mathrm{TiO_2}$–$\mathrm{Cu/H2O}$ hybrid nanofluid transport dependent on shape factor in MHD stagnation point flow, Powder Technology 322 (2017) 428–438. https://doi.org/10.1016/j.powtec.2017.09.006

[17] Ghadimi, A., Saidur, R., Metselaar, H., A review of nanofluid stability properties and characterization in stationary conditions, International Journal of Heat and Mass Transfer 54 (17–18) (2011) 4 051–4 068. https://doi.org/10.1016/j.ijheatmasstransfer.2011.04.014

[18] Guedri, K., Khan, A., Gul, T., Mukhtar, S., Alghamdi, W., Yassen, M. F., Tag Eldin, E., Thermally dissipative flow and entropy analysis for electromagnetic trihybrid nanofluid flow past a stretching surface, ACS Omega 7 (37) (2022) 33 432–33 442. https://doi.org/10.1021/acsomega.2c04047

[19] Gul, T., Saeed, A., Nonlinear mixed convection couple stress tri-hybrid nanofluids flow in a Darcy-Forchheimer porous medium over a nonlinear stretching surface, Waves in Random and Complex Media (2022) 1–18. https://doi.org/10.1080/17455030.2022.2077471

[20] Hale, N., Moore, D., A sixth-order extension to the MATLAB package *bvp4c* of J. Kierzenka and L. Shampine, Report No. 08/04, Oxford University Computing Laboratory, 2008.

[21] Hamad, M. A. A., Analytical solution of natural convection flow of a nanofluid over a linearly stretching sheet in the presence of magnetic field, International Communications in Heat and Mass Transfer 38 (4) (2011) 487–492. https://doi.org/10.1016/j.icheatmasstransfer.2010.12.042

[22] Hazarika, S., Ahmed, S., Chamkha, A. J., Analysis of platelet shape $\mathrm{Al_2O_3}$ and $\mathrm{TiO_2}$ on heat generative hydromagnetic nanofluids for the base fluid $\mathrm{C_2H_6O_2}$ in a vertical channel of porous medium, Walailak Journal of Science and Technology 18 (14) (2021) No. 21424. https://doi.org/10.48048/wjst.2021.21424

[23] Hosseinzadeh, S., Hosseinzadeh, K., Hasibi, A., Ganji, D. D., Thermal analysis of moving porous fin wetted by hybrid nanofluid with trapezoidal, concave parabolic and convex cross sections, Case Studies in Thermal Engineering 30 (2022) No. 101757. https://doi.org/10.1016/j.csite.2022.101757

[24] Khan, W. A., Pop, I., Boundary-layer flow of a nanofluid past a stretching sheet, International Journal of Heat and Mass Transfer 53 (11–12) (2010) 2 477–2 483. https://doi.org/10.1016/j.ijheatmasstransfer.2010.01.032

[25] Li, S., Puneeth, V., Saeed, A. M., Singhal, A., Al-Yarimi, F. A. M., Khan, M. I., Eldin, S. M., Analysis of the Thomson and Troian velocity slip for the flow of ternary nanofluid past a stretching sheet, Scientific Reports 13 (1) (2023) No. 2340. https://doi.org/10.1038/s41598-023-29485-0

[26] Manjunatha, S., Puneeth, V., Gireesha, B. J., Chamkha, A. J., Theoretical study of convective heat transfer in ternary nanofluid flowing past a stretching sheet, Journal of Applied and Computational Mechanics 8 (4) (2022) 1 279–1 286. https://doi.org/10.22055/JACM.2021.37698.3067

[27] Masuda, H., Ebata, A., Teramae, K., Hishinuma, N., Alteration of thermal conductivity and viscosity of liquid by dispersing ultra-fine particles. Dispersion of Al_2O_3, SiO_2 and TiO_2 ultra-fine particles, Netsu Bussei 7 (4) (1993) 227–233. https://doi.org/10.2963/jjtp.7.227

[28] Menni, Y., Chamkha, A. J., Massarotti, N., Ameur, H., Kaid, N., Bensafi, M., Hydrodynamic and thermal analysis of water, ethylene glycol and water-ethylene glycol as base fluids dispersed by aluminum oxide nano-sized solid particles, International Journal of Numerical Methods for Heat & Fluid Flow 30 (9) (2020) 4 349–4 386. https://doi.org/10.1108/HFF-10-2019-0739

[29] Mishra, A., Thompson and Troian slip effects on ternary hybrid nanofluid flow over a permeable plate with chemical reaction, Numerical Heat Transfer, Part B: Fundamentals (2024) 1–29. https://doi.org/10.1080/10407790.2024.2346929

[30] Moghimi, S. M., Hosseinzadeh, K., Hasibi, A., Investigation of nanofluid flow in the channel under effect of magnetic field and joule heating, Case Studies in Thermal Engineering 55 (2024) No. 104152. https://doi.org/10.1016/j.csite.2024.104152

[31] Mousavi, S. M., Esmaeilzadeh, F., Wang, X. P., Effects of temperature and particles volume concentration on the thermophysical properties and the rheological behavior of $CuO/MgO/TiO_2$ aqueous ternary hybrid nanofluid: Experimental investigation, Journal of Thermal Analysis and Calorimetry 137 (2019) 879–901. https://doi.org/10.1007/s10973-019-08006-0

[32] Nadeem, S., Ahmad, S., Khan, M. N., Mixed convection flow of hybrid nanoparticle along a Riga surface with Thomson and Troian slip condition, Journal of Thermal Analysis and Calorimetry 143 (2021) 2 099–2 109. https://doi.org/10.1007/s10973-020-09747-z

[33] Navier, L., Memoir on the laws of fluid motion, Mémoires de l'Académie Royale des Sciences 6 (1827). (in French)

[34] Odagiri, H., Advance of science-based industries and the changing innovation system of Japan, In: Asia's Innovation Systems in Transition, (eds.) B.-Å. Lundvall, P. Intarakumnerd, J. Vang, Edward Elgar Publishing, 2006, pp. 200–226. https://doi.org/10.4337/9781847201737

[35] Pal, D., Mondal, H., Hydromagnetic convective diffusion of species in Darcy-Forchheimer porous medium with non-uniform heat source/sink and variable viscosity, International Communications in Heat and Mass Transfer 39 (7) (2012) 913–917. https://doi.org/10.1016/j.icheatmasstransfer.2012.05.012

[36] Reddy Gorla, R. S., Sidawi, I., Free convection on a vertical stretching surface with suction and blowing, Applied Scientific Research 52 (1994) 247–257. https://doi.org/10.1007/BF00853952

[37] Rooman, M., Saeed, A., Shah, Z., Alshehri, A., Islam, S., Kumam, P., Suttiarporn, P., Electromagnetic trihybrid Ellis nanofluid flow influenced with a magnetic dipole and chemical reaction across a vertical surface, ACS Omega 7 (41) (2022) 36 611–36 622. https://doi.org/10.1021/acsomega.2c04600

[38] Shampine, L., Solving a hard BVP with bvp4c, Private communication, Southern Methodist University, Dallas, 2004.

[39] Shampine, L. F., Singular boundary value problems for ODEs, Applied Mathematics and Computation 138 (1) (2003) 99–112. https://doi.org/10.1016/S0096-3003(02)00111-X

[40] Shampine, L. F., Reichelt, M. W., Kierzenka, J., Solving boundary value problems for ordinary differential equations in MATLAB with *bvp4c*, Tutorial notes, 2000, pp. 1–27.

[41] Suresh, S., Venkitaraj, K. P., Selvakumar, P., Chandrasekar, M., Synthesis of Al_2O_3–Cu/ water hybrid nanofluids using two step method and its thermo physical properties, Colloids and Surfaces A: Physicochemical and Engineering Aspects 388 (1-3) (2011) 41–48. https://doi.org/10.1016/j.colsurfa.2011.08.005

[42] Takreem, M. K., Narayana, S. P. V., Impact of Cattaneo-Christov heat flux on mixed convection flow of a ternary hybrid (Cu–Al_2O_3–TiO_2/H_2O) nanofluid over an elongated sheet: A comparative analysis, Indian Journal of Chemical Technology 31 (1) (2024) 57–69. https://doi.org/10.56042/ijct.v31i1.3263

[43] Thakur, A., Sood, S., Tri-hybrid nanofluid flow towards convectively heated stretching Riga plate with variable thickness, Journal of Nanofluids 12 (4) (2023) 1 129–1 140. https://doi.org/10.1166/jon.2023.1990

[44] Thompson, P. A., Troian, S. M., A general boundary condition for liquid flow at solid surfaces, Nature 389 (1997) 360–362. https://doi.org/10.1038/38686

[45] Tlili, I., Shahmir, N., Ramzan, M., Kadry, S., Kim, J.-Y., Nam, Y., Lu, D., A novel model to analyze Darcy Forchheimer nanofluid flow in a permeable medium with entropy generation analysis, Journal of Taibah University for Science 14 (1) (2020) 916–930. https://doi.org/10.1080/16583655.2020.1790171

[46] Turkyilmazoglu, M., Naganthran, K., Pop, I., Unsteady MHD rear stagnation-point flow over off-centred deformable surfaces, International Journal of Numerical Methods for Heat & Fluid Flow 27 (7) (2017) 1 554–1 570. https://doi.org/10.1108/HFF-04-2016-0160

[47] Venkateswarlu, B., Chavan, S., Joo, S. W., Kim, S. C., Selvaraj, M., Thermal impacts of electromagnetic trihybrid nanofluid flow through a porous expanding sheet with chemical amalgamation: Entropy analysis, Case Studies in Thermal Engineering 52 (2023) No. 103721. https://doi.org/10.1016/j.csite.2023.103721

[48] Xin, X., Saeed, A. M., Al-Yarimi, F. A. M., Puneeth, V., Narayan, S. S., The flow analysis of Williamson nanofluid considering the Thompson and Troian slip conditions at the boundary, Numerical Heat Transfer, Part A: Applications 85 (12) (2024) 1 937–1 953. https://doi.org/10.1080/10407782.2023.2212922

[49] Xuan, Y., Li, Q., Heat transfer enhancement of nanofluids, Elsevier International Journal of Heat and Fluid Flow 21 (1) (2000) 58–64. https://doi.org/10.1016/S0142-727X(99)00067-3

[50] Yu, W., France, D. M., Routbort, J. L., Choi, S. U. S., Review and comparison of nanofluid thermal conductivity and heat transfer enhancements, Heat Transfer Engineering 29 (5) (2008) 432–460. https://doi.org/10.1080/01457630701850851